Multi-layer Quasi Three-dimensional Equivalent Model of Axial-Flux Permanent Magnet Synchronous Machine

Mingjie He, Weiye Li, Jun Peng, and Jiangtao Yang

Abstract—**Axial-flux permanent magnet synchronous machine (AFPMSM) enjoys the merits of high torque density and high efficiency, which make it one good candidate in the direct-drive application. The AFPMSM is usually analyzed based on the three-dimensional finite element method (3D FEM) due to its three-dimensional magnetic field distribution. However, the 3D FEM suffers large amount of calculation, time-consuming and is not suitable for the optimization of AFPMSM. Addressing this issue, a multi-layer quasi three-dimensional equivalent model of the AFPMSM is investigated in this paper, which could take the end leakage into consideration. Firstly, the multi-layer quasi three-dimensional equivalent model of the AFPMSM with single stator and single rotor is derived in details, including the equivalent processes and conversions of structure dimensions, motion conditions and electromagnetic parameters. Then, to consider the influence of end leakage on the performance, a correction factor is introduced in the multi-layer quasi three-dimensional equivalent model. Finally, the proposed multi-layer quasi three-dimensional equivalent model is verified by the 3D FEM based on an AFPMSM under different structure parameters. It demonstrates that the errors of flux linkage and average torque obtained by the multi-layer quasi three-dimensional equivalent model and 3D FEM are only around 2% although the structure parameters of the AFPMSM are varied. Besides, the computation time of one case based on the multi-layer quasi three-dimensional equivalent model is only 6 min, which is much less than that of the 3D FEM, 1.8 h, under the same conditions. Thus, the proposed multi-layer quasi three-dimensional equivalent model could be used to optimize the AFPMSM and much time could be saved by this method compared with the 3D FEM.**

Index Terms—**Axial flux, equivalent model, end leakage, permanent magnet machine.**

I. INTRODUCTION

THE permanent magnet synchronous machine (PMSM) has attracted much attention and developed rapidly in the past

Mingjie He, Weiye Li and Jun Peng are with the CRRC Zhuzhou Institute CO., LTD., Zhuzhou, China (e-mail: mingjiehe_hust@foxmail.com, pengjun@csrzic.com , liwy@csrzic.com).

Jiangtao Yang is with the College of Electrical and Information Engineering, Hunan University, Changsha, China (e-mail: yangjiangtao@hnu.edu.cn).

few decades, during which various topologies have been proposed and investigated, including surface-mounted PMSM, interior PMSM, doubly salient PMSM, flux-switching PMSM, flux-reverse PMSM, axial-flux PMSM (AFPMSM), etc. [1]-[7]. Compared with other PMSMs, the AFPMSM has shorter axial length and is more suitable for the application of wind power generator, in-wheel drive machine of electric vehicle, household appliances, etc. Besides, the AFPMSM enjoys the merits of high torque density and high efficiency. Thus, the AFPMSM has attracted more and more attention in engineering and academic field.

The research on AFPMSM mainly focuses on the enhancing of torque density, reduction of cogging torque, improvement of constant power operating range and reduction of core loss. [8]-[16]. A spoke-type AFPMSM with sinusoidal rotor segment is proposed in [8] to enhance the torque density. By combining radial and axial flux machines together, a novel AFPMSM is proposed and the analysis method is investigated in [9]. It demonstrates that the power and torque densities of the proposed AFPMSM could be improved. To reduce the torque ripple and cogging torque of AFPMSM, several new topologies and methods have been proposed [10]-[13]. A single-stator double-rotor AFPMSM with variable flux is studied in [14] and good flux weakening ability could be obtained by this structure. To improve the constant power operation range, several hybrid-excited AFPMSMs are proposed and investigated in [15, 16].

The AFPMSM suffers three-dimensional magnetic field distribution and it causes that the precise calculation of performance is rather difficult. Though the three-dimensional finite element method (3D FEM) could be used to analyze the AFPMSM, it is not suitable for the optimizing due to that the calculation amount is rather large and it is time consuming. Thus, the equivalent magnetic network model and analytical model of the AFPMSM have been investigated [17-26]. The equivalent magnetic network model of a single-stator double-rotor AFPMSM with coreless stator is investigated in [17]. However, the local saturation of stator iron core can't be considered effectively. The expressions of torque, inductance and size equation of the flux-switching AFPMSM with single stator and double rotors are studied in [18,19]. The analytical model of the AFPMSM with surface-mounted PMs is derived based on the Maxwell equations in [20,21]. The magnetic scalar potential and Bessel functions are introduced to calculate the flux density distribution of the air-cored AFPMSM with

Halbach PMs in [22]. The air-gap magnetic field analytical model of the stator-coreless AFPMSM with single stator and double rotors are derived in [23-26]. However, the analytical methods above mentioned can't take the saturation of iron core into consideration and the calculation accuracy is inevitably poor, especially for the high-saturated AFPMSM.

To facilitate the analysis of AFPMSM and ensure the calculation accuracy, the quasi three-dimensional equivalent model can be used [27]. However, the effect of end leakage on the flux linkage, back electromagnetic force (back EMF) and torque are usually ignored, which may deteriorate the calculation accuracy. To solve this problem, this paper has studied the multi-layer quasi three-dimensional equivalent model with the end leakage taken into consideration based on a single-stator and single-rotor AFPMSM.

The organization of this paper is as follows. In Section II, the topology and operation principle of the single-stator and single-rotor AFPMSM are analyzed. In Section III, the establish processes of the multi-layer quasi three-dimensional equivalent model are given. Besides, the conversions of structure dimensions, movement speed and electromagnetic parameters between the AFPMSM and equivalent model are also derived in this section. In Section IV, the correction factor, permeance of PM, permeance of air gap, leakage permeance between PMs, leakage permeance between PM and rotor, and end leakage permeance are derived in details. In Section V, the effectiveness of the proposed multi-layer quasi three-dimensional equivalent model is verified. Finally, the conclusions are drawn in Section VI.

II. TOPOLOGY AND OPERATION PRINCIPLE

A. Topology

Compared with traditional radial-flux PMSM (RFPMSM), the direction of air-gap flux for the AFPMSM is parallel to the axial direction. Fig. 1 (a) shows the 3D structure of an AFPMSM with single stator and rotor. The combination of stator slots/rotor poles is 24/20. As shown by Fig. 1 (b), the fractional slot concentrated winding is adopted for the AFPMSM. Therefore, the rectangular slot is used to obtain higher slot fill factor, as illustrated by Fig. 1 (b). Fig. 1 (c) shows the structure of rotor and it could be found that the fan-shaped permanent magnet (PM) is used.

B. Operation Principle

The operation principle of AFPMSM is similar with that of the RFPMSM. Sinusoidal flux linkage and back electromotive force (EMF) could be produced in the armature winding with the rotation of rotor, as given by Fig. 2. Thus, the stable
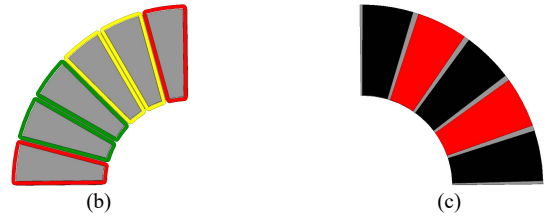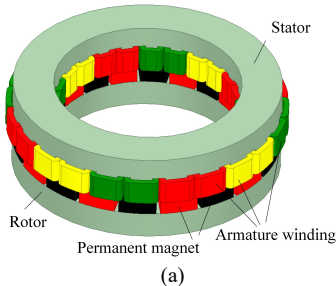

Fig. 1. Topology of the 24/20 AFPMSM. (a). Three-dimensional structure. (b). Stator core and winding. (c). Rotor core and PMs.

electromagnetic torque can be produced when the sinusoidal current is injected into the armature winding. However, the intrinsic 3D flux distribution of the AFPMSM is different with that of the RFPMSM. To obtain the distribution of magnetic flux density of the AFPMSM, the quarter model with 6 stator slots and 5 PM poles are used in the analysis. The boundary condition of the quarter model is set as rotation periodic boundary and the periodicity is set as antiperiodic due to that the number of PM poles in the quarter model is odd. Fig. 3 (a) shows the distribution of magnetic flux density in the stator tooth of AFPMSM. It demonstrates that the flux densities of stator tooth near the ends of inner and outer diameters are different. The flux density of stator tooth near the end of inner diameter is higher. Besides, there are much end leakage flux at the ends of inner and outer diameters, as shown in Fig. 3 (b).
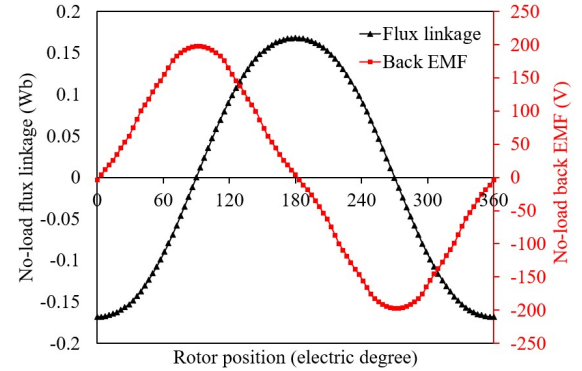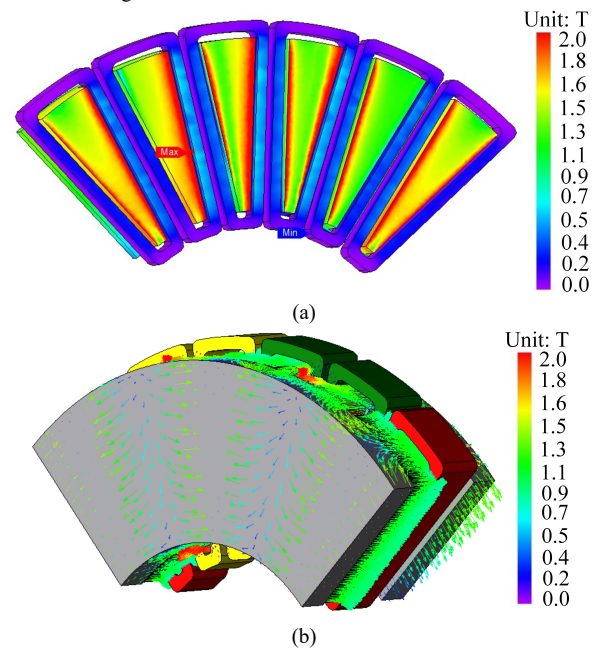

Fig. 2. Flux linkage and back EMF of the AFPMSM.

Fig. 3. Magnetic field distribution of AFPMSM. (a). Flux density distribution. (b). Flux path.

III. Quasi Three-Dimensional Equivalent Model

The 3D FEM is usually adopted to analyze the performance of AFPMSM due to its three-dimensional magnetic field distribution. While the 3D FEM suffers large amount of calculation and time-consuming, and it is not suitable for the optimization of AFPMSM. To solve this problem, the multi-layer quasi three-dimensional equivalent model, which divide the AFPMSM into several layers along the radial direction and use two-dimensional FEM (2D FEM) to calculated the performance of each layer, is proposed and used to facilitate the analysis of AFPMSM in this paper. Moreover, the multi-layer quasi three-dimensional equivalent model could take the end leakage into consideration. Thus, more precise analysis results could be obtained by this equivalent model.

A. Equivalent Process

The equivalent process of the multi-layer quasi three-dimensional equivalent model is illustrated in Fig. 4. The main steps of the equivalent process are given as follows.

Step1: Divide the AFPMSM into several layers along the radial direction. Thus, each layer could be regarded as a small AFPMSM.

Step2: Unfold each layer along the circumference direction and several linear machines with three-dimensional structures can be obtained.

Step3: Establish the two-dimensional equivalent models for the linear machines obtained by Step2, as shown in Fig. 5.

Step4: Analyze the performance indexes of the linear machines using 2D FEM based on the two-dimensional equivalent models established in Step3. Then, the performance indexes of the AFPMSM can be obtained by adding those of the linear machines together.

It should be known that the saturation degrees of the stator tooth near the inner and outer diameters are different, as shown in Fig. 3 (a). Therefore, the number of layers divided along the radial direction for the AFPMSM should be large enough to consider the effect of saturation of stator tooth. The influence of the equivalent model under different number of layers on the calculation results are investigated in Section V.
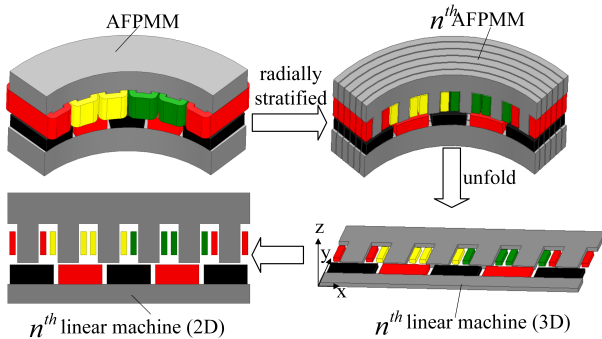

Fig. 4. Equivalent process of the quasi three-dimensional equivalent model.
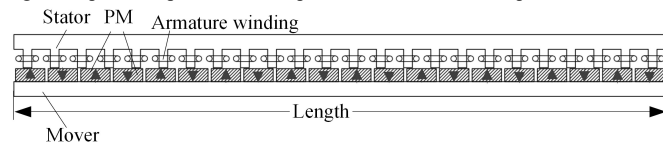

Fig. 5. Equivalent linear machine.

B. Conversion of Structure Parameters

The structure parameters of the AFPMSM may vary along the radial direction, eg. stator tooth width and circumferential length of different layers. Thus, the structure parameters of the equivalent AFPMSMs and linear machines for different layers obtained in step1 and step2 may be different.

The rectangular stator slot is used for the AFPMSM investigated in this paper, so the widths of stator slot for the equivalent AFPMSMs and linear machines at different layers are the same. Besides, the length of air gap, height of stator tooth, height of PM, thicknesses of the stator and rotor yokes for the equivalent AFPMSMs and linear machines are also the same.

Assuming that the AFPMSM is divided into N layers, the depth along the radial direction for the equivalent linear machine of layer n can be calculated by

$$L_{Depth} = \frac{R_o - R_i}{N} \tag{1}$$

where R_i and R_o are the inner and outer radiuses of the AFPMSM, respectively.

As illustrated in Fig. 6, the inner and outer radiuses of the equivalent AFPMSM of layer n can be expressed as

$$\begin{cases} R'_{i\_n} = R_i + (n-1)\dfrac{R_o - R_i}{N} \\ R'_{o\_n} = R_i + n\dfrac{R_o - R_i}{N} \end{cases} \tag{2}$$

The length of the equivalent linear machine of layer n can be regarded as the circumferential length of the corresponding equivalent AFPMSM and could be calculated by

$$L_{length} = \pi(R'_{o\_n} + R'_{i\_n}) \tag{3}$$

The width of stator tooth for the equivalent linear machine of layer n can be calculated by

$$W_{st\_n} = \tau_{s\_n} - W_{ss} \tag{4}$$

where W_{ss} is the width of stator slot, τ_{s_n} is the stator pole pitch of the equivalent linear machine for layer n and can be expressed by

$$\tau_{s\_n} = \frac{\pi(R'_{o\_n} + R'_{i\_n})}{N_s} \tag{5}$$

where N_s is the number of stator slot.

The fan-shaped PM is used for the AFPMSM, so the pole arc coefficients of PMs for different layers are the same. While the widths of PMs are different due to that the inner and outer radiuses of different layers are not the same. The width of PM for the equivalent linear machine of layer n can be calculated by

$$W_{pm\_n} = \tau_{r\_n}\alpha_{pm} \tag{6}$$

where α_{pm} is the pole arc coefficients of PM, τ_{r_n} is the rotor pole pitch of layer n and can be expressed by

$$\tau_{r\_n} = \frac{\pi(R'_{o\_n} + R'_{i\_n})}{N_r} \tag{7}$$

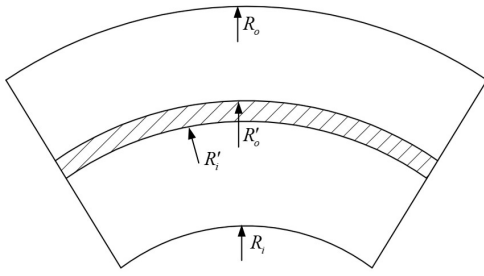where N_r is the number of rotor poles.

Fig. 6. The equivalent inner and outer diameters for the nth-layer AFPMSM.

C. Conversion of Motion and Electromagnetic Parameters

To analyze the performance of the AFPMSM of layer n using the corresponding equivalent linear machine, the rotation speed of AFPMSM must be converted into motion speed, as given by

$$S_{M\_n} = \frac{\pi S_R}{60}(R'_{o\_n} + R'_{i\_n}) \qquad (8)$$

where S_{M_n} is the motion speed of the equivalent linear machine of layer n, S_R is the rotation speed of the equivalent AFPMSM of layer n, which is the same with that of the AFPMSM.

The electric period of the equivalent linear machine of layer n is the same with that of the AFPMSM and can be expressed by

$$T_{period} = \frac{1}{N_r}\frac{60}{S_R} \qquad (9)$$

The flux linkage and back EMF of the equivalent linear machine of layer n are also the same with those of the corresponding AFPMSM. Thus, the flux linkage and back EMF of the AFPMSM can be obtained by summing those of the equivalent linear machines of all layers together, and can be expressed by

$$\begin{cases} \psi'_A = \sum_{n=1}^{N} \psi_{A\_n} \\ E'_0 = \sum_{n=1}^{N} E_{0\_n} \end{cases} \qquad (10)$$

where ψ'_A and E'_0 are the A-phase flux linkage and back EMF of the AFPMSM, ψ_{A_n} and E_{0_n} are the A-phase flux linkage and back EMF of the equivalent linear machine of layer n.

The electromagnetic torque of the equivalent AFPMSM of layer n can be calculated by

$$T_n = \frac{R'_{o\_n} + R'_{i\_n}}{2}F_n \qquad (11)$$

where T_n is the electromagnetic torque of the equivalent AFPMSM of layer n and F_n is the electromagnetic force of the equivalent linear machine of layer n.

Thus, the electromagnetic torque of the AFPMSM can be obtained by

$$T' = \sum_{n=1}^{N} T_n \qquad (12)$$

IV. CORRECTION FACTOR AND CALCULATION OF LEAKAGE PERMEANCE

The end leakage flux can't be considered when the performance of the AFPMSM is calculated by the 2D FEM based on the equivalent linear machines described in Section III. Thus, the calculated results based on the equivalent linear machines would be larger than those of the AFPMSMs. To obtain more accurate performance indexes, including flux linkage, back EMF, average torque, etc., a correction factor, which could take the effect of end leakage flux into consideration, is introduced in the quasi three-dimensional equivalent model.

A. Correction Factor

The magnetic circuit of one PM pole for the AFPMSM is illustrated in Fig. 7 (a). Defining F_{pm} as the magnetomotive force of PM, Λ_{pm}, Λ_g and Λ_{end} as the permeances of PM, air gap and end leakage magnetic circuit under one PM pole, respectively, Λ_{mm} as the leakage permeance between the adjacent PMs, Λ_{mr} as the leakage permeance between the PM and rotor yoke of one side, Φ_{pm}, Φ_{end} and Φ_g as the total flux, end leakage flux and air-gap flux under one PM pole, respectively.

Based on Fig. 7 (a), it could be found that the magnetic circuits of the PM in the middle are closed through the adjacent two PMs. Defining the right half of the PM in the middle as PM_{rm} and the left half of the PM at the right as PM_{lr}. The magnetic circuit of PM_{rm} is closed through the PM_{lr}, as illustrated by the red line in Fig. 7 (a). Therefore, the corresponding equivalent magnetic circuit of PM_{rm} and PM_{lr} can be modelled as Fig. 7 (b). It is known that the permeances of the PM_{rm} and PM_{lr}, permeances of the air gap and end leakage magnetic circuit corresponding to the PM_{rm} and PM_{lr} are only half of the corresponding permeance under one PM pole due to that the area of the magnetic circuit is reduced by half, as shown by Fig. 7 (b). Considering that the magnetomotive force of PM is only related to the coercivity of the PM material and the thickness of the PM, the magnetomotive forces of the PM_{rm} and PM_{lr} are both equal to F_{pm}.

For the leakage permeance between the adjacent PMs, Λ_{mm}, as illustrated in Fig. 7 (b), it could be regards as connected in series of two permeances, whose values are both equal to $2\Lambda_{mm}$, as shown in Fig. 7 (c). Based on the theory of magnetic circuit, it could be found that the magnetic potentials of the two points at both sides of the dotted line in Fig. 7 (c) are equal to each other. Thus, the Fig. 7 (c) could be simplified as Fig. 7 (d). Fig. 7 (e) is the simplified equivalent model by ignoring the end leakage flux magnetic circuit.

Based on Figs. 7 (d) and (e), the correction factor considering the effect of end leakage flux is defined and can be calculated by

$$K_{end} = \frac{\Phi_g}{\Phi'_g} = \frac{\Lambda_{pm}+\Lambda_g+2\Lambda_{mr}+4\Lambda_{mm}}{\Lambda_{pm}+\Lambda_g+2\Lambda_{mr}+4\Lambda_{mm}+\Lambda_{end}} \qquad (13)$$
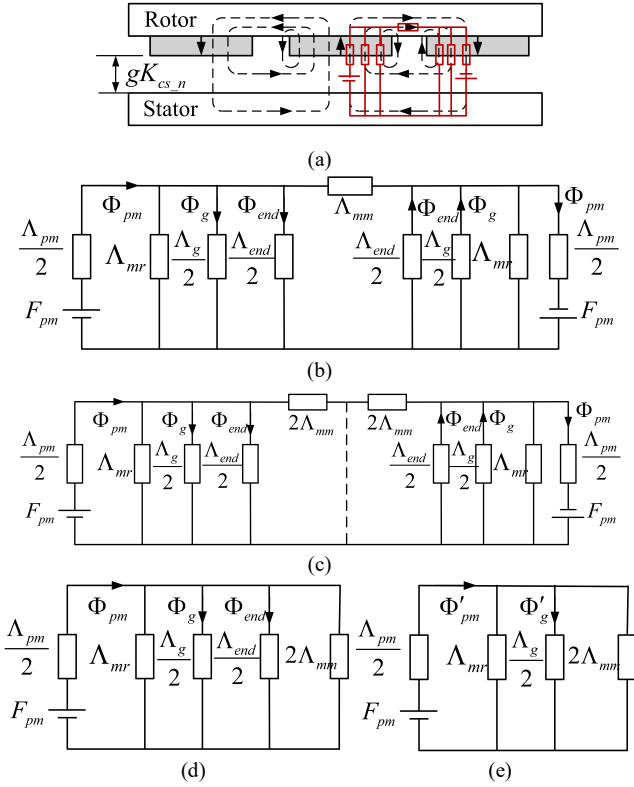
Fig. 7. Magnetic circuit of PM and the equivalent model. (a). Magnetic circuit. (b). Equivalent model I. (c). Equivalent model II. (d). Simplified equivalent model. (e). Simplified equivalent model by ignoring the end leakage flux circuit.

Thus, the flux linkage, back EMF and average torque considering the effect of end leakage for the AFPMSM can be obtained by

$$
\begin{cases}
\psi_A = \psi'_A K_{end} \\
E_0 = E'_0 K_{end} \\
T = T' K_{end}
\end{cases}
\tag{14}
$$

Based on (13), it could be found that the permeance Λ_{pm}, Λ_g, Λ_{end}, Λ_{mm} and Λ_{mr} should be obtained to calculate the correction factor. The line-arc equivalent magnetic circuit model is used to calculate the relevant permeance.

B. Permeance of PM

The permeance of PM for the equivalent AFPMSM of layer n can be expressed as

$$
\Lambda_{pm\_n} = \frac{\mu_r \mu_0 \tau_{r\_n} \alpha_{pm} L_{Depth}}{H\_PM}
\tag{15}
$$

where μ_r is the relative permeability of PM, μ_0 is the vacuum permeability, and H_PM is the height of PM.

The PM permeances for the equivalent AFPMSMs of different layers can be regarded as parallel with each other. Thus, the permeance of PM for the AFPMSM can be obtained and given as

$$
\Lambda_{pm} = \sum_{n=1}^{N} \Lambda_{pm\_n}
\tag{16}
$$

C. Permeance of Air Gap

To facilitate the calculation of air-gap permeance, the stator

slot is equivalent to a smooth surface by Carter coefficient. The Carter coefficient for the equivalent AFPMSM of layer n can be expressed by

$$
K_{cs\_n} = \frac{\tau_{s\_n}}{\tau_{s\_n} - W_{ss} + \frac{4g}{\pi} \ln\left(1 + \frac{\pi}{4g} W_{ss}\right)}
\tag{17}
$$

where g is the actual length of air gap.

Thus, the air-gap permeance corresponding to one PM pole can be calculated by

$$
\Lambda_{g\_n} = \frac{\mu_0 \tau_{r\_n} \alpha_{pm} L_{Depth}}{g K_{cs\_n}}
\tag{18}
$$

The air-gap permeances for the equivalent AFPMSMs of different layers can be regarded as parallel with each other. Therefore, the total air-gap permeance of the AFPMSM corresponding to one PM pole can be obtained as

$$
\Lambda_g = \sum_{n=1}^{N} \Lambda_{g\_n}
\tag{19}
$$

D. Leakage Permeance between PMs

The leakage magnetic circuit between adjacent PMs is equivalent to the line-arc model, as shown in Fig. 8. Thus, the leakage permeance between the adjacent PMs for the equivalent AFPMSM of layer n can be expressed as

$$
\Lambda_{mm\_n} = \int_0^{g K_{cs\_n}} \frac{\mu_0 L_{Depth}}{\pi x + \tau_{r\_n}(1 - \alpha_{pm})} dx
\tag{20}
$$

The leakage permeance between the adjacent PMs of different layers can be regarded as parallel with each other. Therefore, the total leakage permeance between the adjacent PMs can be obtained as

$$
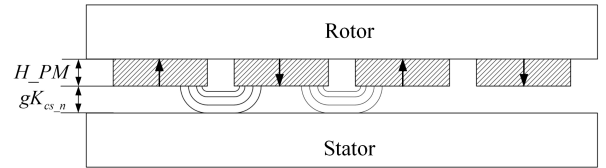\Lambda_{mm} = \sum_{n=1}^{N} \Lambda_{mm\_n}
\tag{21}
$$

Fig. 8. Leakage magnetic circuit between the adjacent PMs.

E. Leakage Permeance between PM and Rotor

As shown in Fig. 9, the length of leakage magnetic circuit between the PM and rotor yoke could be regarded as the sum of a semicircle and line. Thus, the line-arc model is used to calculate the leakage permeance. The leakage permeance between the PM and rotor yoke for the equivalent AFPMSM of layer n are given by

$$
\Lambda_{mr\_n} = \int_0^{L_{mr}} \frac{\mu_0 L_{Depth}}{\pi x + H\_PM} dx
\tag{22}
$$

where L_{mr} is the upper limit of integral and can be obtained by

$$
L_{mr} = \min\left(\frac{(1 - \alpha_{pm})\tau_{r\_n}}{2}, g K_{cs\_n}\right)
\tag{23}
$$

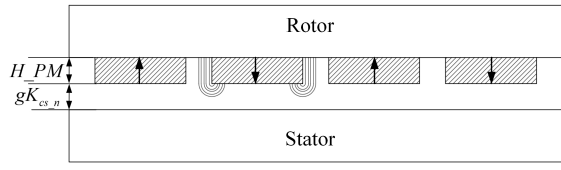Thus, the leakage permeance between the PM and rotor yoke for the AFPMSM could be obtained by

$$\Lambda_{mr} = \sum_{n=1}^{N} \Lambda_{mr\_n} \qquad (24)$$

Fig. 9. Leakage magnetic circuit between the PM and rotor yoke.

F. End Leakage Permeance

For the AFPMSM, the PM may form closed magnetic circuit at the ends of inner and outer diameter, which would lead to end leakage flux and make the flux through the air gap reduced. The end leakage magnetic circuit are illustrated by Fig. 10. The line-arc model is used to calculate the end leakage permeance, as given by

$$\begin{cases} \Lambda_{end\_i} = \int_0^{\frac{2\pi}{N_r}\alpha_{pm}} \int_0^{gK_{cs\_1}} \dfrac{\mu_0 R_i}{\frac{3}{2}\pi x + H\_PM} dx d\theta \\[4mm] \Lambda_{end\_o} = \int_0^{\frac{2\pi}{N_r}\alpha_{pm}} \int_0^{gK_{cs\_N}} \dfrac{\mu_0 R_o}{\frac{3}{2}\pi x + H\_PM} dx d\theta \end{cases} \qquad (25)$$

where K_{cs_1} and K_{cs_N} are the Carter coefficients considering the effect of stator slot for the innermost and outermost equivalent linear machines.

Considering that the integral function has nothing to do with the circumferential position angle θ, the expression of the end leakage permeance (25) can be simplified as

$$\begin{cases} \Lambda_{end\_i} = \dfrac{2\pi\alpha_{pm}R_i}{N_r} \int_0^{gK_{cs\_1}} \dfrac{\mu_0}{\frac{3}{2}\pi x + H\_PM} dx \\[4mm] \Lambda_{end\_o} = \dfrac{2\pi\alpha_{pm}R_o}{N_r} \int_0^{gK_{cs\_N}} \dfrac{\mu_0}{\frac{3}{2}\pi x + H\_PM} dx \end{cases} \qquad (26)$$
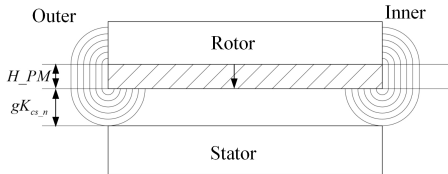

Fig. 10. The end leakage magnetic circuit.

As illustrated by Fig. 10, the permeances of end leakage magnetic circuits are parallel with each other and the total end leakage permeance could be calculated by

$$\Lambda_{end} = \Lambda_{end\_i} + \Lambda_{end\_o} \qquad (27)$$

Therefore, the correction factor K_{end} could be obtained by substituting (16), (19), (21), (24), (26) and (27) to (13). Then, the flux linkage, back EMF and torque of the AFPMSM can be calculated by (14). It is known that the correction factor K_{end} is related with the structure parameters of the AFPMSM and the number of layers, N. Based on the structure parameters given in Table I, the correction factor K_{end} can be calculated and is equal to 0.988 when the number of layers is four, which means the end leakage flux of the AFPMSM investigated in this paper

is at a relatively low level.

V. Verification

To verify the effectiveness of the proposed multi-layer quasi three-dimensional equivalent model, the comparison of the flux linkage and average torque calculated by the proposed equivalent model and 3D FEM is made under different structure parameters. Besides, the influence of the number of layers, N, on the calculation results is also analyzed and compared.

The main structure and design parameters of the AFPMSM are illustrated and given in Fig. 11 and Table I, respectively. To facilitate the comparison, the flux linkage and average torque are converted into unit value in the following analysis. The base values of flux linkage and average torque are 0.1873 Wb and 41.76 N·m, respectively, which are obtained by 3D FEM based on the design parameters given in Table I. It should be known that the thermal load of the AFPMSM is kept the same during the analysis.
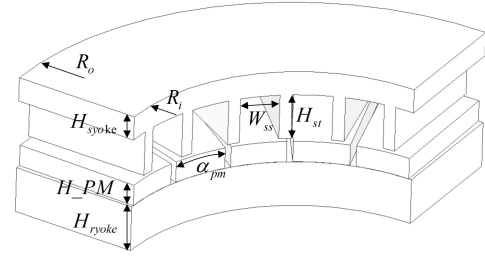

Fig. 11. Structure parameters of the AFPMSM

TABLE I
MAIN DESIGN PARAMETERS OF THE AFPMSM

Symbol	Description	Value	Unit
N_s	Number of stator slot	24	-
N_r	Number of rotor poles	20	-
R_o	Outer radius	100	mm
R_i	Inner radius	50	mm
g	Length of air gap	0.5	mm
W_{ss}	Width of stator slot	10	mm
H_{st}	Height of stator tooth	15	mm
H_PM	Height of PM	7	mm
α_{pm}	Pole embrace of PM	0.9	-
H_{syoke}	Height of stator yoke	8	mm
H_{ryoke}	Height of rotor yoke	8	mm

A. Ai-gap length

The flux linkage and average torque under different air-gap lengths are calculated by the multi-layer quasi three-dimensional equivalent model and 3D FEM, as given by Figs. 12 (a) and (b). It demonstrates that the flux linkage and torque obtained by both the equivalent model and 3D FEM decrease with the increasing of airgap length, which is mainly caused by the increasing of air-gap reluctance. Besides, it could be found that the difference between the results calculated by the equivalent model and 3D FEM tends to be smaller with the increasing of number of layers N. While the number of layers N increases to more than four, the difference would no longer decrease significantly. The flux linkage and torque errors between the results calculated by the equivalent model and 3D FEM are given in Figs. 12 (c) and (d), which indicates that the error would be smaller than 2% when the number of layers N is
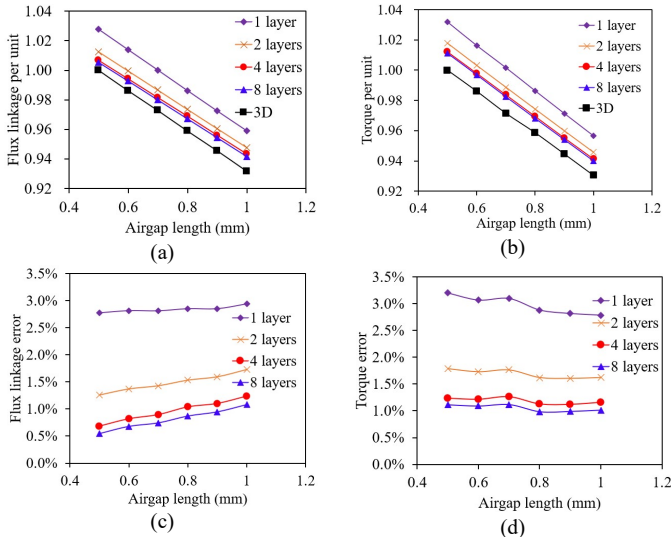
Fig. 12. Flux linkage and torque versus air-gap length curves. (a). Flux linkage. (b). Torque. (c). Flux linkage error. (d). Torque error.

larger than four.

B. Split Ratio

The split ratio of the AFPMSM is defined by the ratio of inner and outer radiuses, as given by

$$K_{splitratio} = \frac{R_i}{R_o} \qquad (28)$$

Thus, the flux linkage and average torque under different split ratio based on the equivalent model and 3D FEM are analyzed and given by Figs. 13 (a) and (b). It is shown that the flux linkage and torque would decrease with the increasing of split ratio, which is quite different with those of the RFPMSM. Besides, it could be found that the results obtained by the equivalent model would be closer to those of 3D FEM when the number of layers N is more than four. Figs. 13 (c) and (d) show that the flux linkage and average torque errors between the results calculated by the equivalent model and 3D FEM, which demonstrates that the errors are smaller than 3% when the number of layers N is larger than four.
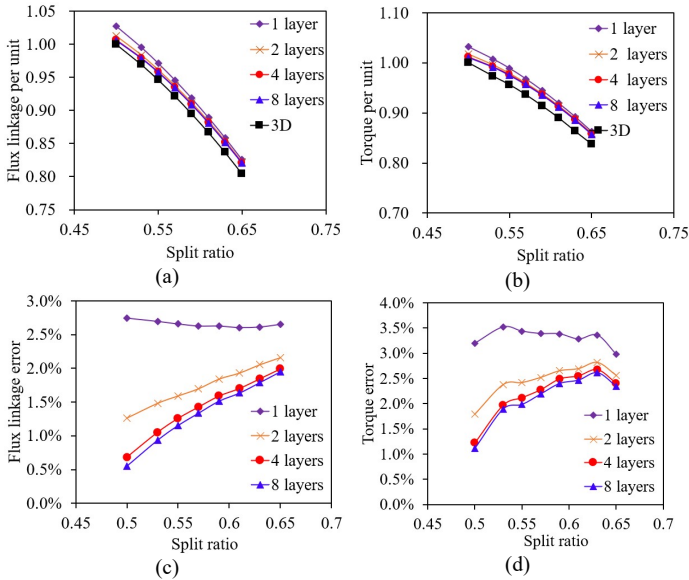

Fig. 13. Flux linkage and torque versus split ratio curves. (a). Flux linkage. (b). Torque. (c). Flux linkage error. (d). Torque error.

C. Pole Arc Coefficient of PM

The flux linkages and average torques of the AFPMSM with different pole arc coefficients of PM calculated by the equivalent model and 3D FEM are given by Fig. 14 (a) and (b), which demonstrates that the flux linkage and average torque obtained by the two methods would both increase with the increasing of pole arc coefficient of PM. Besides, it could be found that the flux linkage and average torque calculated by the equivalent model decrease with the increasing of number of layers N. The flux linkage and average torque errors between both methods are given by Fig. 13 (c) and (d), respectively. It indicates that the errors would be smaller than 2% when the number of layers N is larger than four.
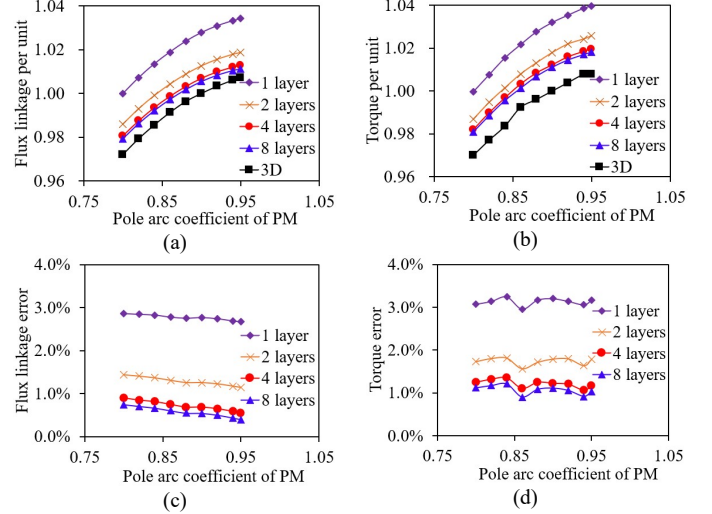

Fig. 14. Flux linkage and torque versus pole embrace of PM curves. (a). Flux linkage. (b). Torque. (c). Flux linkage error. (d). Torque error.

D. Height of PM

The flux linkage and average torque versus the height of PM curves are given by Fig. 15 (a) and (b) respectively. It shows that the flux linkage and average torque would both increase with the height of PM increasing, which is mainly caused by the increasing of air-gap flux density. Besides, the calculated results based on the equivalent model would become smaller with the number of layers N increasing and are closer to those of obtained by 3D FEM. The flux linkage and average torque errors between the equivalent model and 3D FEM would be smaller than 3% when the number of layers N is beyond four, as given by Fig. 15 (c) and (d).

E. Width of Stator Slot

The flux linkages under different widths of stator slot are analyzed based on the equivalent model and 3D FEM, as given by Fig. 16 (a). It indicates that the flux linkage decreases with the increasing of stator slot width due to that the equivalent air-gap length is increased. However, the torque would increase first and then decrease with the increasing of stator slot width, which is mainly caused by the increasing of current. Besides, it demonstrates that the calculated results based on the equivalent model are closer to those of obtained by the 3D FEM when the number of layers N is larger than four. Moreover, the flux linkage and average torque errors are smaller than ± 2% when the number of layers N is larger than four, as given by Fig. 16 (c) and (d).
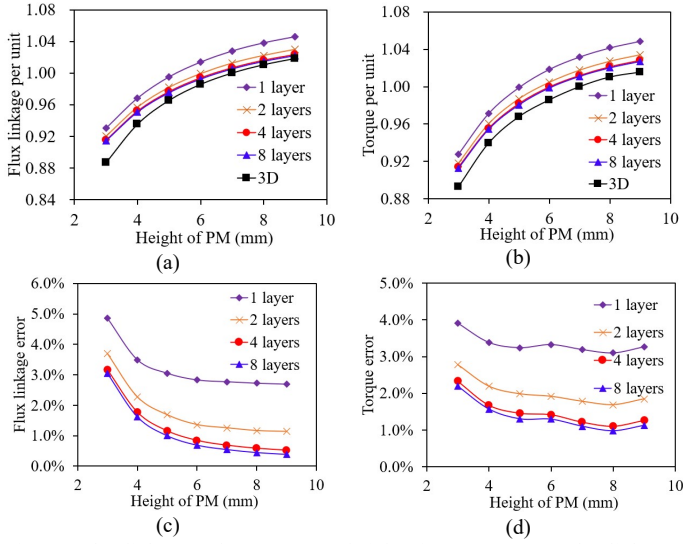
Fig. 15. Flux linkage and torque versus height of PM curves. (a). Flux linkage. (b). Torque. (c). Flux linkage error. (d). Torque error.
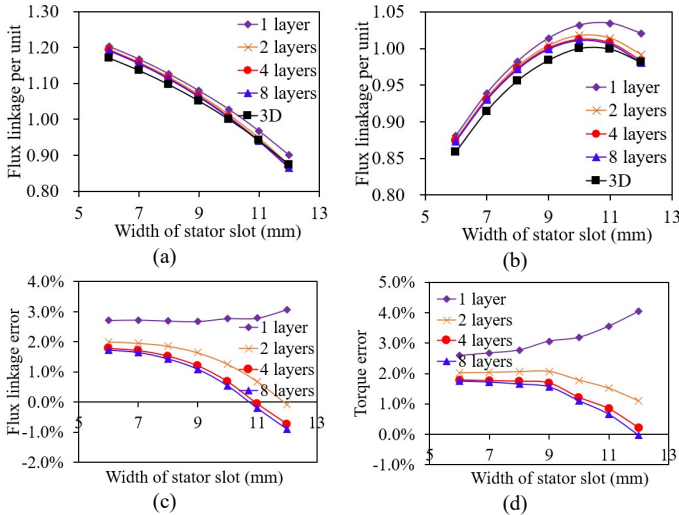

Fig. 16. Flux linkage and torque versus width of stator slot curves. (a). Flux linkage. (b). Torque. (c). Flux linkage error. (d). Torque error.

F. Height of Stator Tooth

Fig. 18 (a) shows the flux linkages under different height of stator tooth and it indicates that the flux linkage decreases with the increasing of stator tooth height slightly. However, the area of stator slot would become larger with the increasing of stator tooth height, which causes the current increasing due to that the thermal load is constant. Thus, the average torque would increase with the increasing of stator tooth height, as given by Fig. 17 (b). Besides, it could also be found that the flux linkage and average torque calculated by the equivalent model are closer to those of obtained by 3D FEM when the number of layers N is beyond four, and the errors are less than 3%, as shown in Fig. 17 (c) and (d).

G. Torque and Losses

To further verify the effectiveness of the proposed multi-layer quasi three-dimensional equivalent model, the cogging torque, average torque, torque ripple and losses of the AFPMSM are analyzed, and the number of layers is set as four. The main design parameters are given in Table I and the analy-
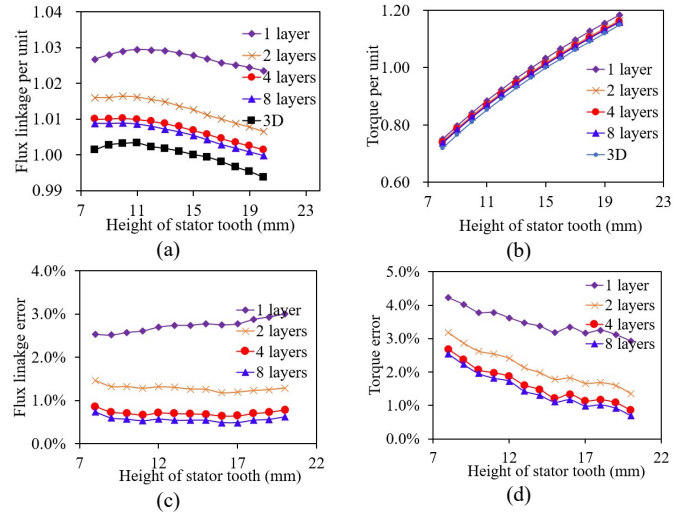

Fig. 17. Flux linkage and torque versus height of stator tooth curves. (a). Flux linkage. (b). Torque. (c). Flux linkage error. (d). Torque error.

sis results are given in Fig. 18. The cogging torques obtained by the proposed equivalent model and 3D FEM are 1.3 N·m and 1.7 N·m, respectively. It could be found that the error of cogging toques calculated by the two methods is relatively high. As given by Fig. 18 (a), the average torque calculated by the proposed equivalent model, 41.8 N·m, is almost the same with that of calculated by 3D FEM, 41.3 N·m. However, the peak-to-peak torques obtained by the proposed equivalent model and 3D FEM are 0.89 N·m and 1.49 N·m, respectively, which demonstrates that large errors may be caused when the proposed equivalent model is used to calculate the torque ripple of AFPMSM.

Fig. 18 (b) shows the core losses and PM eddy-current losses of the AFPMSM. The core losses calculated by the proposed equivalent model and 3D FEM are almost the same, which are 28.5 W and 28.0 W, respectively. However, the PM eddy-current losses obtained by 3D FEM, 70.5 W, is much higher than that calculated by the equivalent model, 10.4 W. The reason is that the PMs are divided into several parts for the proposed multi-layer quasi three-dimensional equivalent model and the eddy-current path is also cut.

H. Computation Time

The computation time of a case based on the multi-layer quasi three-dimensional equivalent model and 3D FEM is given in Table II. It is known that the system of computer is
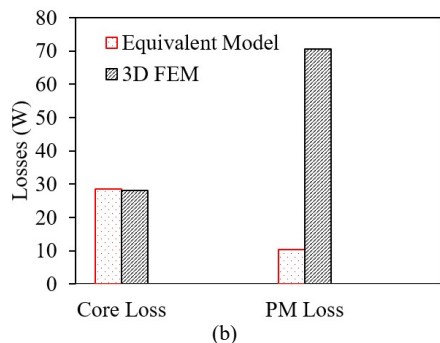

(a)
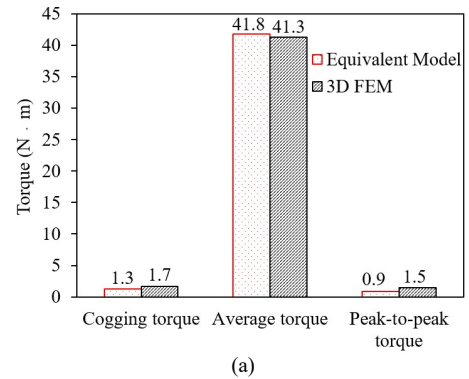
Fig. 18. Comparison of torque and losses. (a). Torque. (b). Losses.

Inter(R) Xeon(R) Gold 6240 CPU with 500G RAM. The grid quantity of the 3D FEM and equivalent model is 646,900 and 39,286, respectively. As shown in Table II, the computation time for the equivalent model is about 6 min, which is much less than that of the 3D FEM, 1.8 h.

TABLE II
SIMULATION TIME

Method	System	Computation time of a single transient solve	Grid quantity
3D FEM	Inter(R) Xeon(R) Gold 6240 CPU with 30 cores used and 500G RAM	About 1.8 h	646,900
The equivalent model with four layers		About 6 min	39,286

Therefore, the multi-layer quasi three-dimensional equivalent model proposed in this paper could predict the flux linkage and average torque correctly although the design parameters of the AFPMSM are varied. Moreover, the errors between the results calculated by the multi-layer quasi three-dimensional equivalent model and 3D FEM are only around 2%. Thus, the proposed multi-layer quasi three-dimensional equivalent model can be used to optimize the AFPMSM and it is time saving compared with the 3D FEM.

VI. CONCLUSION

This paper has proposed and investigated the multi-layer quasi three-dimensional equivalent model of the AFPMSM with single stator and single rotor. Firstly, the operation principle of the AFPMSM is introduced briefly. Then, the equivalent process, conversions of main structure dimensions, motion conditions and electromagnetic parameters between the multi-layer quasi three-dimensional equivalent model and AFPMSM are analyzed in details. To consider the effect of the end leakage on the calculation results, a correction factor is introduced and derived based on the equivalent magnetic circuit model. Finally, the proposed multi-layer quasi three-dimensional equivalent model is verified based on a designed AFPMSM. It indicates that the errors between the analysis results obtained by the multi-layer quasi three-dimensional equivalent model and 3D FEM are only around 2% when the number of layers N is larger than four. Besides, the computation time of one case based on the multi-layer quasi three-dimensional equivalent model, 6 min, is much less than that of the 3D FEM, 1.8 h, under the same

conditions. Thus, the proposed multi-layer quasi three-dimensional equivalent model can be used to analyze and optimize the AFPMSM and much time could be saved by this method compared with the 3D FEM. Besides, the multi-layer quasi three-dimensional equivalent model proposed in this paper could also be used to analyze the performance of other AFPMSMs by revising the calculation method of correction factor.

REFERENCES

[1] G. H. Du, W. Xu, J. G. Zhu, N. Huang, "Power loss and thermal analysis for high power high speed permanent magnet machines," *IEEE Trans. Ind. Electron.*, Vol. 67, No. 4, pp. 2722-2733, Apr. 2020.
[2] Y. Wang, J. H. Feng, W. Y. Li, etc. "Calculation of d-axis and q-axis inductances and characteristics of PM motor by global cross-coupling method," Journal of Control and Information Technology, vol. 3, no. 1, pp. 22-26, Jul. 2018.
[3] J. H. Feng, "Key technology and development trend of permanent magnet motor traction system for rail transit," Journal of Electric Drive for Locomotives, vol. 6, no. 1, pp. 9-17, Nov. 2018.
[4] C. Cheng, W. Hua, J. Zhang, and W. Zhang, "Overview of stator permanent magnet brushless machines," *IEEE Trans. Ind. Electron.*, vol. 58, no. 11, pp. 5087–5100, Nov. 2011.
[5] W. Xu, G. Lei, T. Wang, X. Yu, J. Zhu, and Y. Guo, "Theoretical research on new laminated structure flux switching permanent magnet machine for novel topologic plug-in hybrid electrical vehicle," *IEEE Trans. Magn.*, vol. 48, no. 11, pp. 4050-4053, Nov. 2012.
[6] M. He, W. Xu, J. Zhu, etc. "A novel hybrid excited doubly salient machine with asymmetric stator poles," *IEEE Trans. Ind. Appl.*, vol.55, no.5, pp. 4723-4732, Sept. 2019.
[7] F. G. Capponi, G. D. Donato, F. Caricchi, "Recent advances in axial-flux permanent-magnet machine technology," *IEEE Trans. Ind. Appl.*, vol. 48, no. 6, pp. 2190-2205, Nov./Dec. 2012.
[8] M. Aydin, M. Gulec, "A new coreless axial flux interior permanent magnet synchronous motor with sinusoidal rotor segments," *IEEE Trans. Magn.*, vol. 52, no. 7, #8105204, Jul. 2016.
[9] J. M. Seo, J. Ro, S. Rhyu, etc. "Novel hybrid radial and axial flux permanent-magnet machine using integrated windings for high-power density," *IEEE Trans. Magn.*, vol. 51, no. 3, #8100804, Mar. 2015.
[10] T. D. Nguyen, K. Tseng, S. Zhang, etc. "A novel axial flux permanent-magnet machine for flywheel energy storage system: design and analysis," *IEEE Trans. Ind. Electron.*, vol. 58, no. 9, pp. 3784-3794, Sept. 2011.
[11] W. L. Zhao, T. A. Lipo, B. Kwon, "A novel dual-rotor, axial field, fault-tolerant flux-switching permanent magnet machine with high-torque performance," *IEEE Trans. Magn.*, vol. 51, no. 11, #8112204, Nov. 2015.
[12] F. Zhao, T. A. Lipo, B. Kwon, "A novel dual-stator axial-flux spoke-type permanent magnet vernier machine for direct-drive applications," *IEEE Trans. Magn.*, vol. 50, no. 11, # 8104304, Nov. 2014.
[13] M. Shokri, N. Rostami, V. Beehjat, etc. "Comparison of performance characteristics of axial-flux permanent-magnet synchronous machine with different magnet shapes," *IEEE Trans. Magn.*, vol. 51, no. 12, # 8115206, Dec. 2015.
[14] X. Liu, M. Wang, D. Chen, etc. "A variable flux axial field permanent magnet synchronous machine with a novel mechanical device," *IEEE Trans. Magn.*, vol. 51, no. 11, # 8113504, Nov. 2015.
[15] F. G. Capponi, G. D. Donato, G. Borocci, etc. "Axial-flux hybrid-excitation synchronous machine: analysis, design, and experimental evaluation," *IEEE Trans. Ind. Appl.*, vol. 50, no. 5, pp. 3173-3183, Sep./Oct. 2014.
[16] H. Qiu, W. Yu, B. Tang, etc. "Study on the influence of different rotor structures on the axial-radial flux type synchronous machine," *IEEE Trans. Ind. Electron.*, vol. 65, no. 7, pp. 5406-5413, Jul. 2018.
[17] A. Hemeida, A. Lehikoinen, P. Rasilo, etc. "A simple and efficient quasi-3D magnetic equivalent circuit for surface axial flux permanent magnet synchronous machines," *IEEE Trans. Ind. Electron.*, vol. 66, no. 11, pp. 8318-8333, Nov. 2019.
[18] L. Hao, M. Lin, W. Li, etc. "Novel dual-rotor axial field flux-switching

permanent magnet machine," *IEEE Trans. Magn.*, vol. 48, no. 11, pp. 4232-4235, Nov. 2012.

[19] J. H. Kim, Y. Li, BB. Sarlioglu, etc. "Sizing, analysis, and verification of axial flux-switching permanent magnet machine," *IEEE Trans. Ind. Appl.*, vol. 55, no. 4, pp. 3512-3521, Jul./Aug. 2019.

[20] H. Tiegna, A. Bellara, Y. Amara, etc. "Analytical modeling of the open-circuit magnetic field in axial flux permanent-magnet machines with semi-closed slots," *IEEE Trans. on Magn.*, vol. 48, no. 3, pp. 1212-1226, Mar. 2012.

[21] A. Dwivedi, S. K. Singh, R. K. Srivastava, "Analysis and performance evaluation of axial flux permanent magnet motors," *IEEE Trans. Ind. Appl.*, vol. 54, no. 2, pp. 1765-1772, Mar./Apr. 2018.

[22] B. Guo, Y. Huang, F. Peng, "Analytical modeling of manufacturing imperfections in double-rotor axial flux PM machines: effects on back EMF," *IEEE Trans. Magn.*, vol. 53, no. 6, # 7200605, Jun. 2017.

[23] P. Jin, Y. Yuan, Q. Xu, etc. "Analysis of axial-flux Halbach permanent-pagnet machine," *IEEE Trans. Magn.,* vol. 51, no. 11, # 8207404, Nov. 2015.

[24] Y. N. Zhilichev, "Three-dimensional analytic model of permanent magnet axial flux machine," *IEEE Trans. Magn.*, vol. 34, no. 6, pp. 3897-3901, Nov. 1998.

[25] P. Virtic, P. Pisek, M. Hadziselimovic, "Torque analysis of an axial flux permanent magnet synchronous machine by using analytical magnetic field calculation," *IEEE Trans. Magn.*, vol. 45, no. 3, pp. 1036-1039, Mar. 2009.

[26] V. Rallabandi, N. Taran, D. Ionel, "Multilayer concentrated windings for axial flux PM machines," *IEEE Trans. Magn.*, vol. 53, no. 6, # 8103104, Jun. 2017.

[27] Y. Liu, Z. Zhang, W. Geng, etc. "A simplified finite-element model of hybrid excitation synchronous machines with radial/axial flux paths via magnetic equivalent circuit," *IEEE Trans. Magn.*, vol. 53, no. 11, # 7403004, Nov. 2017.

Jun Peng received the B.Eng. degree in mechanical design from Huazhong Agricultural University, Wuhan, China, in 2007, and the M.Sc. degree in electrical engineering from Huazhong University of Science and Technology, Wuhan, China, in 2016.

Since 2007, he has been with CRRC Zhuzhou Institute Co., Ltd., Changsha, China. His major research interests include design and application of permanent magnet machine for electrical vehicle application.

Jiangtao Yang (S'18-M'19) received the B.E. degree from the Wuhan University of Technology, Wuhan, China, in 2014, and the Ph.D. degree from the Huazhong University of Science and Technology, Wuhan, in 2019, both in electrical engineering.

He is currently an Assistant Professor with the College of Electrical and Information Engineering, Hunan University, Changsha, China. His research interests include the design and analysis of high-speed electrical machine, pulsed alternator, and flywheel energy storage system.

Mingjie He received the B.E. degree from the School of Hydropower & Information Engineering, Huazhong University of Science and Technology, Wuhan, China, in 2014. He received the Ph.D. degree with the State Key Laboratory of Advanced Electromagnetic Engineering and Technology, Huazhong University of Science and Technology, China, in 2019.

He is now working at the CRRC Zhuzhou Institute CO., LTD. His current research interest includes the design of doubly salient permanent magnet machine, axial flux permanent magnet machine, hybrid excited machine and magnetic gear.

Weiye Li received the B.E. degree from the School of Automation and Information Engineering, Xi'an University of Technology, Xi'an, China, in 2009. He received the M.E. degree from the School of Electrical Engineering, Xi'an Jiaotong University, Xi'an, China, in 2012.

He has joined the CRRC Zhuzhou Institute CO., LTD from 2012 and he has been engaged in the research and product development of permanent magnet machine.